Cascaded Extended State Observer-Based Speed Controller Design of PMSM Considering Variable Control Gain and Uncertain Disturbance

Shuaipeng Tang, Tingna Shi, *Senior Member, IEEE*, Yanfei Cao, *Member, IEEE*, Yan Yan, and Changliang Xia, *Senior Member, IEEE*

***Abstract*—Aiming at the problems of control gain mismatch and disturbance rejection in permanent magnet synchronous motor control system, this article proposes a variable control gain linear active disturbance rejection controller (VG-LADRC) with strong disturbance rejection ability and control gain adaptive function. This controller adopts a cascaded extended state observer. ESO1 is used to jointly estimate the system control gain and external disturbance, and ESO2 further compensates the residual disturbance on this basis, thus realizing hierarchical processing and coordinated suppression of disturbance observation. To enhance the adaptability of the controller to the change of control gain, this article designs a control gain adaptive law based on error feedback and integrates the motor dynamic information to construct an adaptive factor. Thus, the controller can improve the control gain convergence speed through multidimensional state perception and enhance its robustness under complex working conditions. Theoretical analysis shows that the VG-LADRC has excellent disturbance suppression performance in the range of low-frequency to medium–high frequency and exhibits strong robustness to control gain mismatch. Finally, dynamic tests are carried out to verify the control performance and engineering applicability of the proposed method.**

***Index Terms*—Active disturbance rejection control (ADRC), load disturbance, permanent magnet synchronous motor (PMSM), speed control, variable control gain.**

I. Introduction

PERMANENT magnet synchronous motor (PMSM) has become the core actuator in high-performance motion control fields, such as aerospace servo actuators, industrial robots, and computer numerical control (CNC) machine tools due to its advantages, such as high power density, compact structure, and reliable operation [1], [2]. With the increasing demand for precision control under complex working conditions, the system has put forward more stringent requirements on the robustness, anti-interference, and parameter adaptability of the dynamic speed regulation performance of the motor [3], [4]. However, as a typical nonlinear strong coupling system, the control performance of PMSM is easily restricted by two key factors. The first is the time-varying disturbance during operation, including external disturbances, such as sudden changes in load torque and nonlinear friction of mechanical transmission. The second is the dynamic mismatch of the motor parameters, such as moment of inertia perturbation. Especially under high dynamic conditions, the control gain mismatch caused by the change in moment of inertia will lead to the attenuation of the phase margin of the speed loop. Moreover, the coupling effect of load disturbance and parameter perturbation will further amplify the speed tracking error and even cause system instability [5]. Therefore, for the PMSM-drive system under complex working conditions, it is of great theoretical value and engineering significance to study the speed loop control strategy with both strong anti-interference ability and control gain adaptive characteristics to promote the development of high-performance servo system.

In recent years, many control algorithms have been applied to the field of PMSM speed control and have made significant progress in improving control performance, such as sliding-mode control [6], model predictive control [7], and active disturbance rejection control (ADRC) [8], [9], [10]. Among them, linear active disturbance rejection control (LADRC) has become a research hotspot due to its strong antidisturbance and robustness [11]. Based on the two restrictive factors mentioned above, the current research on the improvement of LADRC can be divided into two major technical branches. The first is disturbance suppression improvement. The steady-state tracking error of the conventional LADRC (C-LADRC) is proportional to the rate of change of the system disturbance. Although the disturbance can be suppressed by increasing the bandwidth of the extended state observer (ESO), this will inevitably amplify the measurement noise [12], [13], [14]. To enhance the anti-interference performance of the C-LADRC at the same bandwidth, Lin et al. [15] proposed a two-degree-of-freedom LADRC based on the improved ESO by changing the feedback channel in the ESO, which improved the suppression ability of low-frequency disturbances. The authors in [16] and [17] designed an adaptive linear/nonlinear switching ADRC method

Received 7 April 2025; revised 3 July 2025; accepted 10 August 2025. Date of publication 13 August 2025; date of current version 22 October 2025. This work was supported in part by the Key Program of National Natural Science Foundation of China under Grant 52237003 and in part by the Zhejiang Leading Innovation and Entrepreneurship Team Project of China under Grant 2024R01012. Recommended for publication by Associate Editor Y. A.-R. I. Mohamed. *(Corresponding author: Tingna Shi.)*

The authors are with the College of Electrical Engineering, Zhejiang University, Hangzhou 310027, China, and also with Zhejiang University Advanced Electrical Equipment Innovation Center, Hangzhou 311107, China (e-mail: tshuaipeng@zju.edu.cn; tnshi@zju.edu.cn; caoyanfei@zju.edu.cn; yan_yan@zju.edu.cn; motor@tju.edu.cn).

Color versions of one or more figures in this article are available at https://doi.org/10.1109/TPEL.2025.3598439.

Digital Object Identifier 10.1109/TPEL.2025.3598439

by combining the advantages of linear and nonlinear ESO. It can automatically adjust the ESO gains according to the tracking error range to maintain strong anti-interference and high-precision tracking performance.

Another technical branch is to increase the adaptive ability of control parameters. Zuo et al. [18] pointed out that in ADRC speed control, when the moment of inertia of the system changes and the control gain coefficient in the controller remains unchanged, the control performance of the system will be greatly reduced. And this performance degradation cannot be compensated by disturbance estimation. We divide the existing research on control gain adaptation into the following two strategies according to the adjustment method. One is the precalibration control gain compensation strategy, which is usually a parameter calibration performed before the system is operated or at a specific stage. And it does not rely on real-time data. Hao et al. [17] use a manual adjustment method to make the control gain in the controller follow the change of the moment of inertia to achieve a better speed regulation effect. In [19], the moment of inertia value is obtained by using the speed information in acceleration and deceleration, and then precalibrates the control gain coefficient. The precalibration strategy reduces the real-time calculation burden through offline optimization, but its static gain setting is difficult to adapt to parameter perturbations under dynamic conditions.

The second is the online observer fusion strategy, which combines multiple observers or algorithms to simultaneously identify system parameters and lumped disturbances [18], [20], [21]. In [6] and [21], according to the mechanical motion equations of PMSM, a combination scheme of moment of inertia identification algorithm based on model reference adaptive system and load torque observation technology based on ESO is designed. The control gain is adaptively adjusted according to the observation results. However, the collaborative work of multiple algorithms often faces challenges in coupling and real-time performance [22]. Furthermore, the extended two-state observer (ETSO) is proposed in [23], which achieves comprehensive compensation for parameter uncertainty by jointly estimating the control gain and lumped disturbance. Based on this, an online self-adjusting speed controller is constructed to improve the speed tracking performance of the system. Although the existing research has made significant progress in speed control under variable control gain and uncertain disturbance conditions, there are still challenges in simultaneously improving the antidisturbance performance and the robustness of the control gain of the controller, which limits its practicality under complex working conditions.

Based on the above challenges, this article proposes a variable control gain LADRC (VG-LADRC) speed controller that combines cascaded ESO (CESO) and control gain adaptive adjustment mechanism. The introduction of the CESO architecture with clear functional division in the VG-LADRC realizes the coordinated estimation of disturbances and control gain. Furthermore, by analyzing the dynamic characteristics of the estimation error and control gain of the ESO1, this article designs an adaptive factor based on error feedback and motor dynamic information, thereby enhancing the real-time adjustment ability of the control system to the changing control gain. This method not only enhances the ability of disturbance rejection but also effectively improves the dynamic response performance of the speed loop under control gain mismatch, providing a robust and adaptive solution for high-performance servo control under complex working conditions.

II. Design of VG-LADRC Speed Controller

In the *dq*-axis reference frame, the voltage equation of PMSM can be expressed as follows:

$$\begin{cases} u_{\mathrm{d}} = Ri_{\mathrm{d}} - L_{\mathrm{q}} i_{\mathrm{q}} p\omega_{\mathrm{m}} + L_{\mathrm{d}} \frac{\mathrm{d}i_{\mathrm{d}}}{\mathrm{d}t} \\ u_{\mathrm{q}} = Ri_{\mathrm{q}} + \left(L_{\mathrm{d}} i_{\mathrm{d}} + \psi_{\mathrm{f}}\right) p\omega_{\mathrm{m}} + L_{\mathrm{q}} \frac{\mathrm{d}i_{\mathrm{q}}}{\mathrm{d}t}. \end{cases} \tag{1}$$

The PMSM control system adopts field-oriented control with $i_{\mathrm{d}}^{*} = 0$. The mechanical motion equation is

$$\dot{\omega}_{\mathrm{m}} = \frac{1}{J}\left(T_{\mathrm{e}} - T_{\mathrm{L}} - B\omega_{\mathrm{m}} - C\mathrm{sgn}\left(\omega_{\mathrm{m}}\right)\right). \tag{2}$$

The electromagnetic torque equation is

$$T_{\mathrm{e}} = \frac{3}{2} p\left(\psi_{\mathrm{f}} + \left(L_{\mathrm{d}} - L_{\mathrm{q}}\right) i_{\mathrm{d}}\right) i_{\mathrm{q}} \tag{3}$$

where u_{d}, u_{q}, i_{d}, i_{q}, L_{d}, and L_{q} are the stator d-axis and q-axis voltages, currents, and inductances, respectively; R is the stator resistance; ψ_{f} is the rotor permanent magnet flux linkage; J is the inertia; B is the viscous friction coefficient; C is the Coulomb friction coefficient; p is the number of pole pairs; ω_{m} is the rotor speed; T_{e} and T_{L} are the electromagnetic torque and the load torque; and $\mathrm{sgn}(x)$ is the sign function.

Let the reference current of the q-axis i_{q}^{*} be the input $u(t)$ of the speed controller; $k_{\mathrm{T}} = 1.5p\psi_{\mathrm{f}}$ be the torque coefficient; and $b(t) = k_{\mathrm{T}}/J$ be the system control gain. Equation (2) can be written as follows:

$$\dot{\omega}_{\mathrm{m}} = b(t)u(t) + b(t)d(t) \tag{4}$$

where $d(t)$ is the lumped disturbance

$$\begin{aligned} d(t) = & -\frac{1}{k_{\mathrm{T}}}\left(k_{\mathrm{T}}\left(i_{\mathrm{q}}^{*} - i_{\mathrm{q}}\right) - 1.5p\left(L_{\mathrm{d}} - L_{\mathrm{q}}\right) i_{\mathrm{d}} i_{\mathrm{q}}\right) \\ & - \frac{1}{k_{\mathrm{T}}}\left(T_{\mathrm{L}} + B\omega_{\mathrm{m}} + C\mathrm{sgn}\left(\omega_{\mathrm{m}}\right)\right). \end{aligned} \tag{5}$$

For the C-LADRC speed controller, timely sensing and compensating for the system lumped disturbance $d(t)$ is the key to maintaining dynamic performance, which is achieved by ESO in the controller. Increasing the observation bandwidth can enhance the estimation performance of the lumped disturbance. However, due to the limitation of the single ESO structure, this will also synchronously amplify the high-frequency noise component in the feedback signal, resulting in an increase in the steady-state fluctuation of the speed tracking error. In addition, the deviation between the control gain $b(t)$ in the controller and the actual system caused by changes in operating conditions (such as motor magnetic saturation or load inertia perturbation) will be directly mapped to the dynamic adjustment of the speed loop, reducing its dynamic response speed.

A. Design of the CESO in VG-LADRC

To address the above problems, the speed controller designed in this article increases the disturbance observation dimension through a CESO structure and introduces a control gain adaptation law mechanism to automatically adjust the controller parameter. The design of VG-LADRC breaks through the performance bottleneck of the C-LADRC speed controller from both the structural and parameter levels.

Set new state variables x_1, x_2, and x_3, $x_1 = \omega_{\mathrm{m}}$, $x_2 = d(t)$, and $x_3 = b(t)$. Since the control frequency is high, the actual load disturbance and the system control gain can be considered to be constant within a control cycle, that is, $\dot{x}_2 = 0$ and $\dot{x}_3 = 0$. And there exist positive constants D_1, D_2, and D_3 such that $|x_2| \le D_1$, $D_2 \le x_3 \le D_3$ [23]. According to (4), the state equation of the motor can be expressed as follows:

$$\dot{x}_1 = x_3 u(t) + x_3 x_2. \tag{6}$$

The proposed VG-LADRC controller consists of two parts: CESO (ESO1 and ESO2) and control law. ESO1 uses $\hat{x}_1$, $\hat{x}_2$, and $\hat{x}_3$ to estimate the state variables x_1, x_2, and x_3, respectively. ESO1 is designed as follows:

$$\begin{cases} e_1 = x_1 - \hat{x}_1 \\ \dot{\hat{x}}_1 = \hat{x}_3 u(t) + \hat{x}_3 \hat{x}_2 + h_1 e_1 \\ \dot{\hat{x}}_2 = h_2 e_1 + \frac{h_2}{h_1}\dot{e}_1 \\ \dot{\hat{x}}_3 = \Phi(\alpha, e_1, u(t), \hat{x}_2) \end{cases} \tag{7}$$

where $h_2\dot{e}_1/h_1$ is the decoupling term, which can eliminate the influence of the speed estimation error e_1 on the extended disturbance term $\hat{x}_2$. It can enhance the antidisturbance performance of the control system. $\Phi(\alpha, e_1, u(t), \hat{x}_2)$ as the control gain adaptive law will be designed and analyzed in detail in the Section II-B.

ESO2 performs in-depth processing on the estimation results of ESO1. It can further improve the estimation accuracy and suppression capability of complex disturbances and improve the robustness and response speed of the control system. ESO2 uses $\hat{z}_1$ and $\hat{z}_2$ to estimate the state variable x_1 and the remaining lumped disturbance $x_3x_2 - \hat{x}_3\hat{x}_2$ in the system, respectively. ESO2 is designed as follows:

$$\begin{cases} e_{\mathrm{z1}} = x_1 - \hat{z}_1 \\ \dot{\hat{z}}_1 = \hat{x}_3 u(t) + \hat{z}_2 + \hat{x}_3 \hat{x}_2 \\ \dot{\hat{z}}_2 = h_4 e_{\mathrm{z1}} + h_3 \dot{e}_{\mathrm{z1}} \end{cases} \tag{8}$$

where h_1, h_2, h_3, and h_4 are the positive observer gain coefficients.

The control law in the controller is designed as

$$u(t) = \frac{u_0 + \dot{x}_1^* - (\hat{z}_2 + \hat{x}_3\hat{x}_2)}{\hat{x}_3} \tag{9}$$

where $u_0 = k_{\mathrm{p}}(x_1^* - x_1)$, k_{p} is the proportional gain coefficient, and $x_1^* = \omega_{\mathrm{m}}^*$ is the speed reference command.

To ensure that the control signal $u(t)$ operates within the actual executable range and reduce over-regulation caused by external disturbances or parameter uncertainties, the output limit value $u_{\max}$ is set so that $u(t) \in [-u_{\max}, u_{\max}]$.

B. Design of Control Gain Adaptive Law

In this section, through analysis of the estimation errors and control gain dynamic characteristics of the ESO1, the control gain dynamic compensation equation is constructed. It can realize the real-time dynamic adjustment of the control gain coefficient. Let $e_2 = x_2 - \hat{x}_2$ be the load disturbance estimation error, and $e_3 = x_3 - \hat{x}_3$ be the control gain observation error. With the help of (6) and (7), the estimation errors of the parameters to be estimated can be obtained

$$\dot{e}_1 = e_3\,(u(t) + \hat{x}_2) + x_3 e_2 - h_1 e_1. \tag{10}$$

According to (10), $x_3e_2 - h_1e_1$ and $\dot{e}_1$ can be regarded as input signals in the control gain adjustment process, and $(u(t) + \hat{x}_2)$ is the convergence characteristic information. Let α be the adjustable coefficient and $\alpha > 0$, the control gain adaptive law can be designed as

$$\Phi(\alpha, e_1, u(t), \hat{x}_2) = \alpha e_3 = \alpha \frac{\dot{e}_1 - x_3 e_2 + h_1 e_1}{u(t) + \hat{x}_2}. \tag{11}$$

Considering that e_2 cannot be directly calculated as an intermediate state variable in the observer, the control gain adaptation law $\dot{\hat{x}}_3 = \Phi(\alpha, e_1, u(t), \hat{x}_2)$ is simplified to

$$\Phi(\alpha, e_1, u(t), \hat{x}_2) = \alpha \frac{\dot{e}_1 + h_1 e_1}{u(t) + \hat{x}_2}. \tag{12}$$

According to (7), $u(t) + \hat{x}_2$ reflects the running state of the estimated speed $\hat{x}_1$. When $\hat{x}_1$ is running in a steady state, $u(t) + \hat{x}_2$ is a variable value fluctuating around zero. At this time, the control gain adaptive law will face the singularity problem, which seriously affects the stability of the system operation. To solve this problem, α is designed as follows:

$$\alpha = \gamma(u(t) + \hat{x}_2)^2 \tag{13}$$

where γ is the adaptive factor $\gamma > 0$.

To improve the practicability of the proposed controller in complex industrial equipment, this article designs adaptive factor based on the actual operating conditions of the motor: First, the control gain mismatch in the controller will reduce the speed tracking performance, induce speed overshoot, or lag. And the performance degradation is positively correlated with the degree of mismatch. Second, large load disturbance $d(t)$ will inevitably slow down the speed tracking effect, leading to increased dynamic fluctuations of the motor and longer adjustment time. This dynamic characteristic will accelerate the convergence process of the estimated control gain that depends on the change of the convergence characteristic information.

Based on the above actual operating conditions, this article designs the adaptive factor based on speed tracking error and load disturbance to improve the convergence speed and robustness of the control gain adaptive law

$$\gamma = \beta \arctan(l_{\mathrm{m}}) \cdot \max\left(0, \mathrm{sgn}(l_{\mathrm{m}} - \varphi)\right) \tag{14}$$

where l_{m} is the absolute value of the speed tracking error; φ is the adaptive threshold, $\varphi > 0$. β is the adjustment factor

$$\beta = \begin{cases} \beta_1, & \text{if } |\hat{x}_2| < \delta \\ \beta_2, & \text{if } |\hat{x}_2| \ge \delta \end{cases} \tag{15}$$

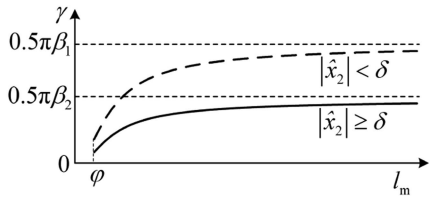

Fig. 1. Adjustment curve of the adaptive factor.

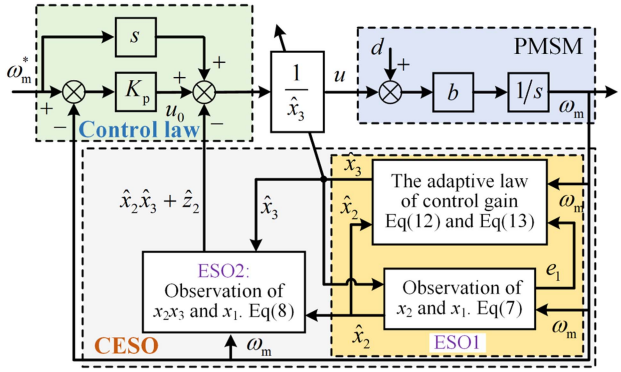

Fig. 2. Schematic diagram of the VG-LADRC speed control.

where β_1 and β_2 are the constants, and $\beta_1 > \beta_2$. δ is the judgment threshold of the switching convergence coefficient. It is recommended to set it to 0.1–0.2 of the rated load torque of the motor, which can effectively balance the relationship between the convergence speed and the system stability.

The adjustment curve of the adaptive factor with speed tracking error and load disturbance is shown in Fig. 1. Compared with the constant coefficient, the variable adaptive factor can autonomously adjust the convergence speed of the control gain according to the actual operating conditions. It can increase the convergence speed when the speed tracking performance is poor or the lumped disturbance is small, and reduce or even stop the convergence when the speed tracking is good. In addition, the use of the arctangent function can limit the adjustment range of γ and effectively avoid the overadjustment behavior of the coefficient.

The deep integration of the control gain adaptive law and the CESO structure enables the controller to autonomously adjust the control parameters according to changes in operating conditions. This design breaks through the limitations of the traditional fixed gain control strategy in dynamic disturbance suppression and parameter adaptability. The cooperative compensation mechanism of gain disturbance significantly improves the system's robustness to multisource disturbances and parameter perturbations, while taking into account the dynamic response speed and steady-state accuracy of the motor speed. The VG-LADRC speed control block diagram is shown in Fig. 2.

C. Stability Analysis of the Speed Controller

Based on the dynamic characteristics and interaction mechanism of VG-LADRC, this section establishes the stability criterion of the closed-loop system to prove its global convergence under disturbance and parameter uncertainty conditions. The obtained results provide theoretical support for the engineering application of the control strategy.

Set the extended state variable $\hat{z}_3$ so that $\hat{z}_2 = \hat{z}_3 + h_3 e_{z1}$, and let $e_{z3} = x_3 x_2 - \hat{x}_3 \hat{x}_2 - \hat{z}_3$. It is reasonable to assume that there are positive constants D_4, D_5, D_6, D_7, D_8, and D_9 such that $|\hat{x}_2| \le D_4$, $\hat{x}_3 \le D_5$, $|\dot{\hat{x}}_{23}| \le D_6$, $\hat{x}_{23} = \hat{x}_2 \hat{x}_3$, $|\hat{z}_3| \le D_7$, $|\dot{\hat{e}}_{z1}| \le D_8$, and $|e_{z1}| \le D_9$ [23]. Combining (6)–(8), the observer error equations are as follows:

$$\begin{cases} \dot{e}_1 = e_3 \left(u(t) + x_2\right) + \hat{x}_3 e_2 - h_1 e_1 \\ \dot{e}_{z1} = e_3 u(t) + e_{z3} - h_3 e_{z1}. \end{cases} \tag{16}$$

Select the Lyapunov function $V_1 = \frac{1}{2}e_1^2 + \frac{1}{2}e_{z1}^2$, we can get

$$\begin{aligned} \dot{V}_1 &= e_1 \dot{e}_1 + e_{z1} \dot{e}_{z1} = e_1 \left(a - h_1 e_1\right) + e_{z1} \left(b - h_3 e_{z1}\right) \\ &\le -h_1 \|e_1\|^2 + \|e_1\| \, \|a\|_{\max} - h_3 \|e_{z1}\|^2 + \|e_{z1}\| \, \|b\|_{\max} \end{aligned} \tag{17}$$

where $a = e_3(u(t) + x_2) + \hat{x}_3 e_2$ and $b = e_3 u(t) + e_{z3}$. $\|\cdot\|$ represents the norm. $\|a\|_{\max}$ and $\|b\|_{\max}$ represent the maximum value of the norm of a and b, $\|a\|_{\max} = (D_5 - D_2)(D_1 + u_{\max}) + D_5(D_1 + D_4)$ and $\|b\|_{\max} = (D_5 - D_2)u_{\max} + D_1 D_3 + D_4 D_5 + D_7$. For the positive-definite function V_1, there exists $\dot{V}_1 < 0$ when $\|e_1\|$ and $\|e_{z1}\|$ are greater than $\max\{\|a\|_{\max}/h_1, \|b\|_{\max}/h_3\}$, which ensures that e_1 and e_{z1} are uniformly ultimately bounded [24].

According to (6)–(8) and (12), the disturbance and control gain estimation error equations are derived as follows:

$$\dot{e}_2 = -h_2 e_1 - \frac{h_2}{h_1} \dot{e}_1 \tag{18}$$

$$\dot{e}_3 = -\alpha \frac{\dot{e}_1 + h_1 e_1}{u(t) + \hat{x}_2} \tag{19}$$

$$\dot{e}_{z3} = -\dot{\hat{x}}_{23} - h_4 e_{z1}. \tag{20}$$

Combining (16) and (18), we can get the load disturbance estimation error

$$\dot{e}_2 = -\frac{h_2}{h_1} \hat{x}_3 e_2 - \frac{h_2}{h_1} e_3 \left(u(t) + x_2\right). \tag{21}$$

Combining (10) and (19), the control gain estimation error is

$$\dot{e}_3 = -\alpha e_3 - \gamma \left(u(t) + \hat{x}_2\right) x_3 e_2. \tag{22}$$

Combining (16) and (20), the residual lumped disturbance estimation error is

$$\dot{e}_{z3} = \frac{h_4}{h_3} \dot{e}_{z1} - \frac{h_4}{h_3} e_3 u(t) - \frac{h_4}{h_3} e_{z3} - \dot{\hat{x}}_{23}. \tag{23}$$

Establish the positive-definite function $V_2 = \frac{1}{2}e_2^2 + \frac{1}{2}e_3^2 + \frac{1}{2}e_{z3}^2$, it can be derived that

$$\begin{aligned} \dot{V}_2 &= -\frac{h_2}{h_1} \hat{x}_3 e_2^2 - \alpha e_3^2 - \frac{h_4}{h_3} e_{z3}^2 - \frac{h_2}{h_1} e_2 e_3 \left(u(t) + x_2\right) \\ &\quad - \gamma e_2 e_3 \left(u(t) + \hat{x}_2\right) x_3 + e_{z3} \left(\frac{h_4}{h_3} \dot{e}_{z1} - \frac{h_4}{h_3} e_3 u(t) - \dot{\hat{x}}_{23}\right) \\ &\le -\frac{h_2}{h_1} D_5 \|e_2\|^2 + \|e_2\| \, \frac{h_2}{h_1} \left(D_5 - D_2\right)\left(D_1 + u_{\max}\right) \end{aligned}$$

$$-\alpha\|e_3\|^2+\|e_3\|\gamma\left(D_4+u_{\max}\right)D_3\left(D_4+D_1\right)$$
$$-\frac{h_4}{h_3}\|e_{z3}\|^2+\|e_{z3}\|\left(\frac{h_4}{h_3}D_8+\frac{h_4}{h_3}\left(D_5-D_2\right)u_{\max}+D_6\right). \tag{24}$$

According to (24), let $f=(1-D_2/D_5)(D_1+u_{\max})$, $g=\gamma(D_4+u_{\max})D_3(D_4+D_1)/\alpha$, and $h=(D_5-D_2)u_{\max}+D_8+D_6h_3/h_4$. For the control gain adaptive law, there are two cases: whether the absolute value of the speed tracking error l_{m} is less than the adaptive threshold φ. First, when $l_{\mathrm{m}}<\varphi$, the adjustable coefficient α is zero, the control gain stops converging, and $\hat{x}_3$ is a constant. There exists $\dot{V}_2\le 0$ when e_2 and e_{z3} are greater than $\max\{f,h\}$. Second, when $l_{\mathrm{m}}>\varphi$, there exists $\dot{V}_2\le 0$ when e_2, e_3, and e_{z3} are greater than $\max\{f,g,h\}$. The above analysis proves the stability of the estimated disturbance and the estimated control gain during the observation process.

Based on the motor control model (6) with the proposed control law (9), in order to prove that the speed tracking error $e=x_1^*-x_1$ is convergent and eventually uniformly bounded, the Lyapunov equation $V_3=e^2/2$ is established, and then

$$\begin{aligned}\dot{V}_3&=e(\dot{x}_1^*-\dot{x}_1)\\&=e(\dot{x}_1^*-\hat{x}_3u(t)-x_3x_2)\\&=e(-k_{\mathrm{p}}\left(x_1^*-x_1\right)+\hat{z}_2+\hat{x}_3\hat{x}_2-x_3x_2)\\&\le -k_{\mathrm{p}}\|e\|^2+\|e\|\left(D_1D_3+D_4D_5+D_7+h_3D_9\right).\end{aligned} \tag{25}$$

There exists $\dot{V}_3<0$ when $\|e\|\ge(D_1D_3+D_4D_5+D_7+h_3D_9)/k_{\mathrm{p}}$.

The above analysis shows that the proposed VG-LADRC speed control system is stable.

III. Performance Analysis of VG-LADRC Speed Controller

A. Convergence Analysis of Estimated Control Gain

According to (21) and (22), the solutions of the control gain and load disturbance estimation error equations are as follows:

$$e_3=C_1e^{\int-\alpha\mathrm{d}t}-\left(\int m_1e^{\int\alpha\mathrm{d}t}\mathrm{d}t\right)e^{\int-\alpha\mathrm{d}t} \tag{26}$$

$$e_2=C_2e^{\int-\frac{h_2\hat{x}_3}{h_1}\mathrm{d}t}-\left(\int m_2e^{\int\frac{h_2\hat{x}_3}{h_1}\mathrm{d}t}\mathrm{d}t\right)e^{\int-\frac{h_2\hat{x}_3}{h_1}\mathrm{d}t} \tag{27}$$

where C_1 and C_2 are the constants, regarded as the initial estimated errors of $\hat{x}_3$ and $\hat{x}_2$; $m_1=\gamma(u(t)+\hat{x}_2)x_3e_2$ and $m_2=h_2e_3(u(t)+x_2)/h_1$ are their respective coupling error terms. Let $q_1=-\alpha$ and $q_2=-h_2\hat{x}_3/h_1$ represent the convergence coefficients of the estimated control gain and load disturbance, respectively. Since q_1 and q_2 are both less than zero, e_2 and e_3 will converge exponentially, which provides a basis for the convergence of $\hat{x}_3$ and $\hat{x}_2$ from the analytical expression.

In practical applications, environmental noise can significantly reduce the convergence accuracy of the estimated control gain. This phenomenon is especially obvious when the motor is in steady state. It can be seen from (26) that the convergence coefficient of the control gain contains the dynamic change information $u(t)+\hat{x}_2$ of the motor. When the motor gradually tends to steady state from dynamic, the convergence coefficient decreases due to the weakening of dynamic information. Then, the convergence performance of the estimated control gain decreases, and the impact of environmental noise on it will be further amplified. The design of the adaptive adjustment mechanism of control gain in this article can effectively suppress this influence. The adjustable coefficient α takes the absolute value of the speed tracking error $\omega_{\mathrm{m}}^*-\omega_{\mathrm{m}}$ as its adaptive condition. When the motor runs in the same dynamic process, it will adaptively adjust the convergence coefficient according to the absolute value of the speed deviation to accelerate the convergence speed of $\hat{x}_3$. When the motor speed tracking performance is good, the appropriate adaptive threshold φ can be designed to pause the convergence of $\hat{x}_3$ when the absolute value of the speed deviation is less than φ. This design effectively blocks the influence of environmental noise disturbance on the steady-state accuracy of the estimated control gain.

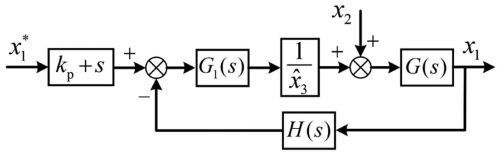

Fig. 3. Simplified block diagram of the VG-LADRC speed control.

B. Analysis of Control System Antidisturbance Performance

This section derives the transfer function and its Bode diagram characteristics under different control gains so as to theoretically analyze the antidisturbance performance of the proposed VG-LADRC and its superiority in structural design.

Let $k_{\mathrm{b}}=\hat{x}_3/x_3$ be the control gain ratio and $G(s)=x_3/s$ be the transfer function of the motor model. According to (7)–(9), the block diagram of the VG-LADRC speed control can be simplified, as shown in Fig. 3. In the figure

$$G_1(s)=\frac{Q(s)\left(s^2+h_3s+h_4\right)}{\left(s^2+h_1s\right)s^2} \tag{28}$$

$$H(s)=k_{\mathrm{p}}+s+\frac{\left(h_2+\frac{h_2}{h_1}s\right)k_{\mathrm{b}}x_3s^3+Q(s)\left(h_4+h_3s\right)s}{Q(s)\left(s^2+h_3s+h_4\right)} \tag{29}$$

where $Q(s)=(s^2+(h_1+h_2k_{\mathrm{b}}x_3/h_1)s+h_2k_{\mathrm{b}}x_3)$.

The tracking transfer function $G_{\mathrm{rvg}}(s)$ and disturbance transfer function $G_{\mathrm{fvg}}(s)$ of the system are as follows:

$$G_{\mathrm{rvg}}(s)=\frac{\left(k_{\mathrm{p}}+s\right)Q(s)\left(s^2+h_3s+h_4\right)}{\left(k_{\mathrm{b}}-1\right)\left(s^2+h_1s\right)s^3+Q_1(s)} \tag{30}$$

$$G_{\mathrm{fvg}}(s)=\frac{k_{\mathrm{b}}\left(s+h_1\right)s^3}{\left(k_{\mathrm{b}}-1\right)\left(s^2+h_1s\right)s^3+Q_1(s)} \tag{31}$$

where $Q_1(s)=Q(s)(k_{\mathrm{p}}+s)(s^2+h_3s+h_4)$.

The proposed VG-LADRC is compared with C-LADRC to evaluate its performance characteristics. Fig. 4 shows the Bode

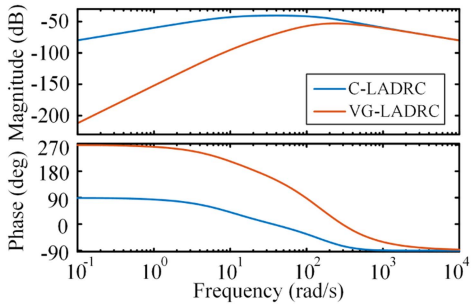

Fig. 4. Bode diagrams of the disturbance transfer function.

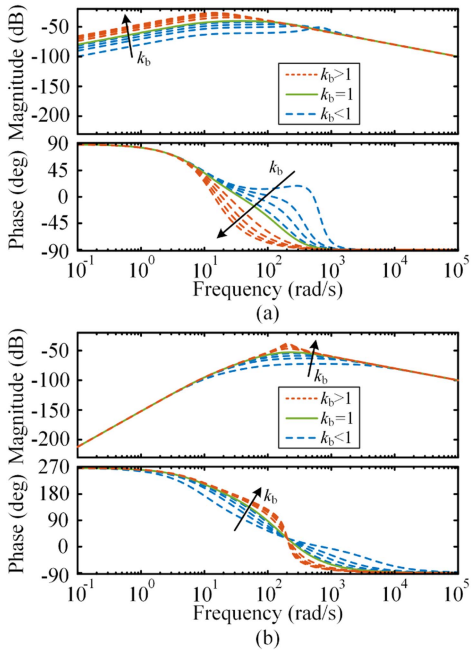

Fig. 5. Bode diagrams of the disturbance transfer function under different k_b. (a) C-LADRC. (b) VG-LADRC.

diagrams of the disturbance transfer function of the two methods without considering the control gain mismatch. Benefiting from the improvement of the observer structure, the proposed VG-LADRC not only significantly outperforms the C-LADRC in low-frequency disturbance suppression, but also shows obvious advantages in medium- and high-frequency disturbance suppression.

Fig. 5 shows the Bode diagrams of the disturbance transfer function of the two methods under different control gain ratios. In contrast, the proposed VG-LADRC has higher robustness to control gain mismatch: when the control gain is mismatched, its low-frequency disturbance suppression performance is almost unaffected, and its high-frequency disturbance suppression performance only changes slightly. However, the C-LADRC has weak anti-interference performance in the whole frequency band due to structural limitations. The above analysis shows that the proposed VG-LADRC significantly improves the antidisturbance capability of the control system under complex working conditions by optimizing the design of the CESO structure. And it can achieve better robustness and control performance without relying on additional algorithms.

In addition, the introduction of the control gain adaptive algorithm will further improve the robustness and control performance of the VG-LADRC. By dynamically adjusting the control gain, the controller can effectively solve the control gain mismatch problem caused by complex operating conditions. While ensuring the stability of low-frequency antidisturbance performance, it can also significantly weaken the impact of control gain changes on high-frequency antidisturbance performance. The addition of the control gain adjustable algorithm enables the proposed controller to exhibit superior anti-interference ability and control accuracy under complex conditions.

C. Design of Control Parameters

It is recommended to adopt the two-stage parameter adjustment strategy of "first ensuring the stable operation of the system, then optimizing the control performance."

1) In the initial tuning stage, to ensure that the system can start smoothly when there is a mismatch in the control gain, it is recommended to set k_{p} to a small value (such as 5–10). In addition, ESO1 needs to jointly estimate the system disturbance and control gain at the same time and has a large dynamic change range. In order to improve the dynamic tracking ability of the actual speed of the motor, it is recommended to set the observer parameter h_1 to a larger initial value. Combining [10] and (21), it can be seen that there is a first-order filtering characteristic between the disturbance observation error value and the coupling error term in ESO1, and the filter cutoff frequency is $h_2\hat{x}_3/h_1$. To ensure that the system has good suppression ability for low-frequency disturbances, the cutoff frequency can be designed to be around 10 rad/s.

ESO2 is mainly responsible for the depth compensation of residual disturbances, and the parameters can be set according to the classical bandwidth tuning method commonly used in C-LADRC. Its parameter design can select $h_4 = (0.5h_3)^2$ to construct an observer channel with moderate bandwidth, effectively enhancing the disturbance observation ability of ESO2 at the medium and high frequency, thereby improving the comprehensive antidisturbance performance of the system.

2) After the motor runs smoothly, start the control gain adaptive mechanism function to further improve the controller's adaptability and dynamic performance under the condition of motor parameter uncertainty. The adaptive threshold φ is the only excitation condition for the algorithm to take effect and exit, and its setting should be set according to the actual speed error amplitude of the motor during steady-state operation.

After the above two-stage parameter setting is completed, the key parameters can be fine-tuned according to the system response to ensure that the controller can effectively estimate the control gain change while suppressing disturbances well. Since the control gain adaptive mechanism is decoupled from the basic control structure module and its functions are independent,

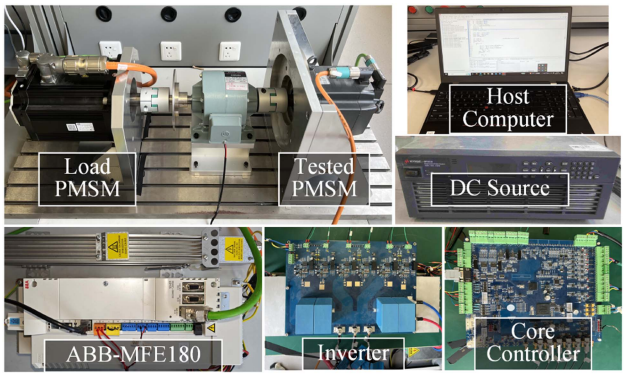

Fig. 6. Diagram of the experimental platform.

TABLE I
PARAMETERS OF THE TESTED PMSM

Parameter	Value	Parameter	Value
Rated power P_N	3.1 kW	Stator resistance R	0.58 Ω
Rated speed n_N	2000 r/min	Flux linkage ψ_f	0.292 Wb
Rated current I_N	6.7 A	d-axis inductance L_d	8 mH
Pole pairs p	4	q-axis inductance L_q	8 mH

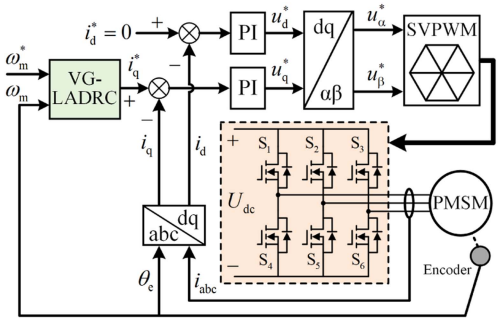

Fig. 7. Block diagram of motor-drive system based on VG-LADRC.

the entire parameter setting process has good executability and physical interpretability, which is suitable for rapid deployment and adjustment in engineering practice.

IV. Experimental Results

This article adopts an experimental platform that can change the control gain and load disturbance, as shown in Fig. 6, to verify the effectiveness of the proposed algorithm. It consists of two PMSMs and an electromagnetic clutch. The tested motor is controlled by a self-developed core controller and inverter, and its parameters are listed in Table I. The ABB driver adjusts the output torque of the loaded motor according to the received instructions and controls the engagement or separation of the electromagnetic clutch. The engagement and separation of the clutch are used to simulate the sudden increase and decrease of system control gain in practical applications.

The experiment adopts the motor-drive system, as shown in Fig. 7. The control system's sampling frequency and carrier frequency are 10 kHz. The proposed controller parameters are set to $k_p = 10$, $h_1 = 8000$, $h_2 = 274$, $h_3 = 400$, $h_4 = 40\,000$, $u_{max} = 12.84$, $\varphi = 0.4$, $\beta_1 = 0.5$, $\beta_2 = 8$, and $\delta = 1.2$. The total moment of inertia of the system when the clutch is separated and engaged are 0.00504 kg·m^2 and 0.01388 kg·m^2, and the corresponding system control gains are 347.6 and 126.2, respectively. Table II summarizes the given speed, load torque, and control gain values of all experiments. To fully demonstrate the superiority of the proposed VG-LADRC in terms of disturbance suppression and control gain dynamic convergence performance, this article compares the proposed method with C-LADRC, cascade ESO-based LADRC (CE-LADRC) [14], and ETSO-based speed controller [23]. The parameters of the compared methods are tuned according to the authors in [14] and [23].

TABLE II
CONFIGURATIONS

Tests	Speed command ω_m^* (rad/s)	Referenced load torque T_L (N•m) and system control gain b
Fig.8 Fig.9	100+30sin(6πt)	$T_L = \begin{cases} 0 & (t \le 10\text{s}) \\ 5 & (10\text{s} < t \le 20\text{s}) \\ 10 & (20\text{s} < t \le 30\text{s}) \\ 0 & (30\text{s} < t \le 40\text{s}) \\ 7 & (40\text{s} < t \le 50\text{s}) \end{cases}$
Fig.10 Fig.11	[(70, 130),250,20]	$b = \begin{cases} 347.6 & (t \le 10\text{s}) \\ 126.2 & (10\text{s} < t \le 30\text{s}) \\ 347.6 & (30\text{s} < t \le 40\text{s}) \\ 126.2 & (40\text{s} < t \le 50\text{s}) \end{cases}$
Fig.12	[(70, 130),250,20]	$T_L = 0, b = 347.6$
Fig.14		$T_L = 7, b = 126.2$
Fig.15	130	$T_L = 3.5 + 3.5\sin(\pi t/2), b = 126.2$

A. Speed Control Performance Under Simultaneous Changes of Control Gain and Load Disturbance

We conducted representative dynamic comparison experiments under different speed instructions to verify the speed control effects of the above four methods when the control gain and lumped disturbance change simultaneously. The experimental condition settings are shown in Table II, where $[(g_d,g_p),t,T]$ represents the trapezoidal speed command, g_p and g_d represent the upper and lower limits of the given command, t is the rise and fall time of the trapezoidal wave, and T represents the waveform change period. The units of time and period are ms and s, respectively.

1) Sinusoidal Speed Command: In order to observe the convergence process of the estimated control gain of the proposed VG-LADRC and ETSO-based speed controller in the initial operation stage, the initial values of the estimated control gain of both are set to 1000. The control gain in C-LADRC and CE-LADRC controllers is set to the system control gain value in the clutch separation state.

The speed tracking results of the four methods are shown in Fig. 8. In the initial stage of motor operation, the motor speed under the four control methods can follow the speed command within 0.4 s. Among them, the VG-LADRC and CE-LADRC with the CESO structure take the shortest time, about 0.28 s.

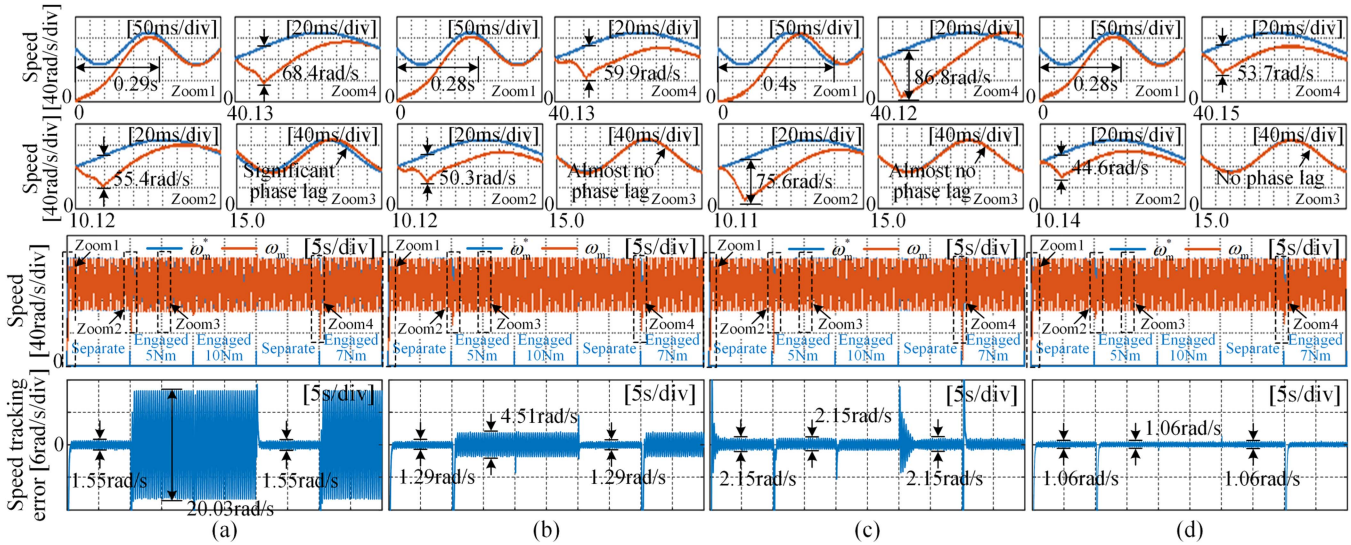

Fig. 8. Speed control effect under sinusoidal speed instructions. (a) C-LADRC. (b) CE-LADRC. (c) ETSO-based speed controller. (d) VG-LADRC.

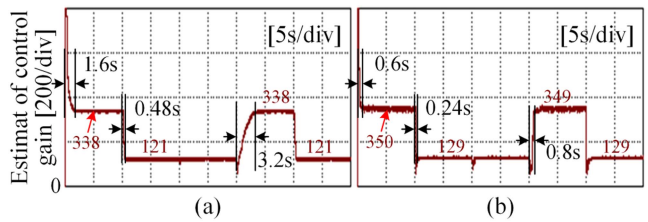

Fig. 9. Convergence results of the estimated control gain. (a) ETSO-based speed controller. (b) VG-LADRC.

The parameter h_1 in ESO1 is set to a larger value to enhance the dynamic tracking capability of the speed observation signal. It can ensure that the controller can obtain motor status information in time under gain mismatch and maintain the basic stability of closed-loop control. Fig. 9 shows the estimated control gain convergence results of the proposed method and the ETSO-based speed controller. In the initial stage, the estimated control gain under the ETSO-based speed controller needs 1.6 s to converge to its actual value. The proposed method benefits from the control gain adaptive law designed based on motor dynamic information and speed tracking error, and it only takes about one-third of the former (0.6 s). Comparing the experimental results under no-load (t<10 s) in Fig. 8, the speed tracking errors of the four methods show significant differences. The C-LADRC is limited by the single observer structure and has poor low-frequency antidisturbance performance, and its speed fluctuation error is 1.55 rad/s. Although the ETSO-based speed controller can adjust the control gain, its disturbance estimation speed is affected by the excitation conditions in the ETSO observer. Even when the control gain in the controller matches the actual system, its speed fluctuation error still reaches 2.15 rad/s, and its antidisturbance performance under no-load is weaker than that of C-LADRC. In comparison, the CE-LADRC with a cascade structure design has improved low-frequency anti-interference performance, and its speed fluctuation error is 1.29 rad/s. The cascaded VG-LADRC has not only improved the disturbance observation dimension, but is also not affected by the disturbance estimation speed. It shows better antidisturbance ability in both low-frequency and medium–high frequency, and its speed fluctuation error is the smallest, which is 1.06 rad/s.

According to Fig. 9, at t = 10 s, the load torque and control gain change simultaneously. At this time, the controller output $u(t)$ and motor dynamic information are prominent, and the convergence characteristics of the estimated control gain in the VG-LADRC and ETSO-based speed controller are obvious. However, due to the use of the filter, the estimated control gain convergence speed of the latter is relatively slow. The time for the two to converge to the system control gain is 0.24 s and 0.48 s, respectively. As the load torque increases to 10 N·m (t = 20 s), the control gain under both control methods can be maintained near the actual value without obvious fluctuations.

In terms of speed control, as shown in Fig. 8, when the load torque and system control gain change simultaneously (t = 10 s), the motor speed under the control of the four controllers shows a significant speed drop. The slower disturbance estimation speed and control gain convergence speed slow down the dynamic response speed of the ETSO-based speed controller, resulting in the largest speed drop of 75.6 rad/s. The proposed VG-LADRC not only has the CESO structure with stronger anti-interference ability but also has the ability to quickly converge the control gain in the controller to its actual value, and its speed drop is the smallest, which is 44.6 rad/s. Even under the condition where only the load torque changes (t = 20 s), the VG-LADRC proposed has almost no speed drop. Comparing the steady-state fluctuation errors of the four methods in Fig. 8 at 10 s<t<30 s, the C-LADRC and CE-LADRC controllers have the largest speed fluctuation due to the mismatch of control gain and have obvious speed lag. With the help of their respective adjustable gain algorithms, VG-LADRC and ETSO-based controller can

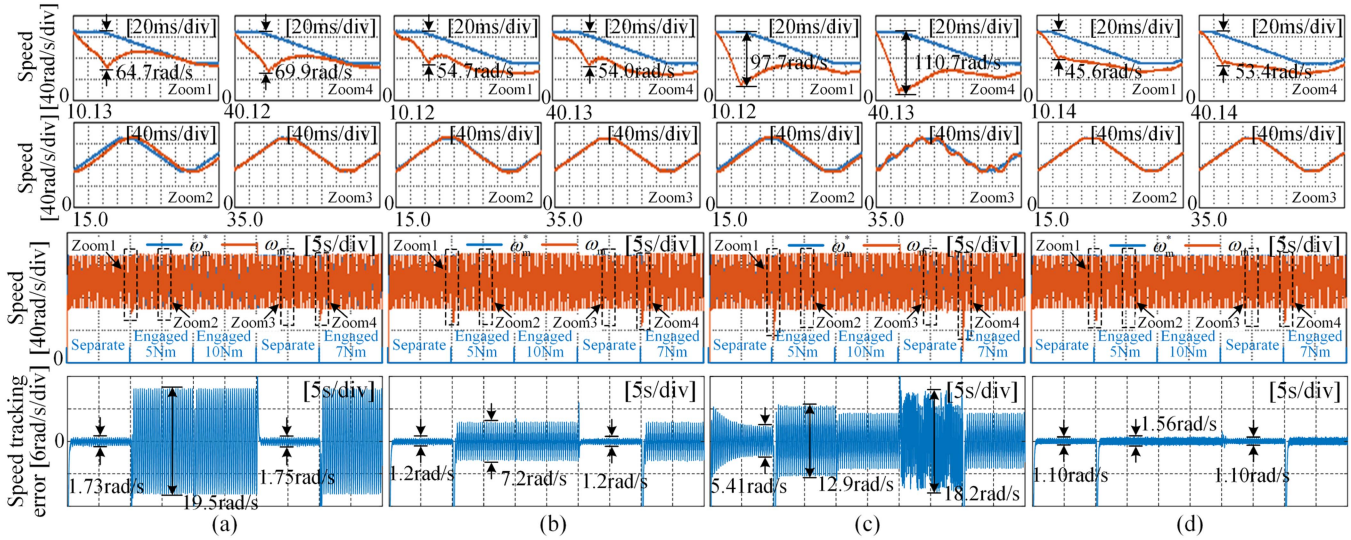

Fig. 10. Speed control effect under trapezoidal speed instructions. (a) C-LADRC. (b) CE-LADRC. (c) ETSO-based speed controller. (d) VG-LADRC.

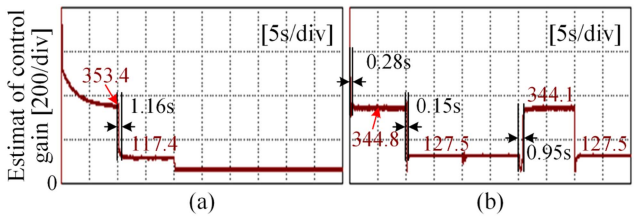

Fig. 11. Convergence results of the estimated control gain. (a) ETSO-based speed controller. (b) VG-LADRC.

maintain the same small speed fluctuation error as no-load conditions.

At $t = 30$ s, the clutch is separated, the load torque suddenly decreases, and the system control gain increases. The sudden decrease in load torque causes the current output in the ETSO-based controller decreases sharply, which weakens the convergence characteristic information of the estimated control gain and slows down its convergence speed. The slower control gain convergence speed makes the ETSO-based controller have a dynamic response speed that exceeds the system itself, causing unnecessary control output fluctuations and speed fluctuations. In contrast, the proposed VG-LADRC uses motor dynamic information as the convergence characteristic information of the control gain, which can capture more details of the motor operation information to improve the convergence speed of the control gain. This allows it to maintain the same level of convergence performance as when the motor is loaded in terms of adjusting the estimated control gain.

2) Trapezoidal Speed Command: The speed tracking results of the four methods under the trapezoidal speed command are shown in Fig. 10. Compared with the sinusoidal speed command in Fig. 8, the rate of change of the trapezoidal speed increases, which puts higher requirements on the rapidity of the control gain adaptive law algorithm. As shown in Fig. 11, the convergence speed of the estimated control gain of the ETSO-based controller is slower than that under the sinusoidal speed command, whether in loaded or no-load conditions. And it even takes about 10 s to converge to the actual system control gain value under no-load condition. In contrast, the proposed method can make the estimated control gain converge to its actual value within no more than 0.3 s.

In addition, we compare the steady-state speed fluctuation errors of the four methods at different times under trapezoidal speed instruction with those under sinusoidal speed instruction. Due to the superiority of the controller structure, the speed fluctuation error under the VG-LADRC control does not increase as significantly as the ETSO-based speed controller, and it is only 1.56 rad/s when loaded.

At $t = 20$ s, the load torque increases from 5 to 10 N·m, and the system control gain remains unchanged. At this time, the motor speed under the control of the ETSO-based controller has a significant speed drop, and its estimated control gain also decreases accordingly. It can be seen from the speed tracking error in Fig. 10 that when the control gain value in the ETSO-based controller is lower than the actual value, the system speed response is accelerated due to the increase in feedback regulation, which causes additional speed fluctuations. However, this fluctuation will cause the rapid jitter of the given current in the controller in a small amplitude range, which seriously affects the stability of the convergence characteristic information of the estimated control gain in the ETSO-based controller, resulting in the failure of the convergence of the estimated control gain in Fig. 11. When the clutch is separated, the parameter mismatch between the estimated controller gain and the actual value is aggravated, which further deteriorates the speed fluctuation. This speed deterioration, in turn, deteriorates the control gain convergence condition and ultimately makes the control gain in the controller unable to converge again after convergence failure.

However, the proposed method can still maintain good speed control performance under trapezoidal speed command. And there is basically no speed drop when the load torque increases

TABLE III
COMPARISON OF ALGORITHM EXECUTION TIME

Execution time	C-LADRC	CE-LADRC	ETSO-based speed control	Proposed VG-LADRC
t_d (s)	0.5e-6	0.79e-6	1.84e-6	1.6e-6

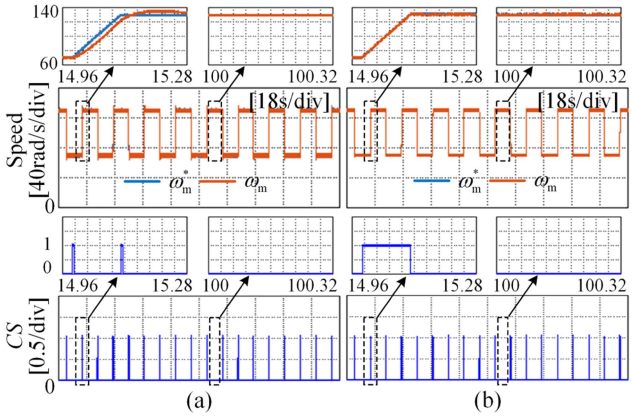

Fig. 12. Speed control effect under no-load. (a) ETSO-based speed controller. (b) VG-LADRC.

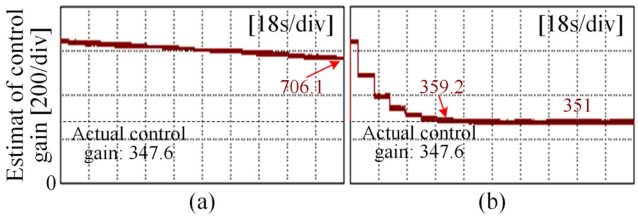

Fig. 13. Convergence results of the estimated control gain under no-load. (a) ETSO-based speed controller. (b) VG-LADRC.

to 10 N·m. And it can still maintain a faster convergence speed and higher convergence accuracy of the control gain under the conditions of clutch separated and re-engagement.

In addition, Table III summarizes the execution time t_d of control methods. Specifically, C-LADRC and CE-LADRC have simple structures and only involve addition, subtraction, and proportional–integral operations, avoiding calling complex function formulae in digital signal processing (DSP). Therefore, their algorithm execution times are short, which are 0.5e-6 s and 0.79e-6 s, respectively. In contrast, the VG-LADRC and the ETSO-based controller both introduce a control gain adaptation mechanism and involve inverse tangent function and hyperbolic tangent function operations. Their computational complexity is relatively high, with execution times of 1.6e-6 and 1.84e-6 s.

It is worth noting that, with the same functions, the execution efficiency of VG-LADRC is improved by about 13% compared with the ETSO-based controller, and it shows better performance in terms of disturbance suppression performance and robustness of control gain convergence. During the experiment, we also measured the execution time of other programs except the speed controller, which is about 1.18e-5 s. From this, it can be calculated that the VG-LADRC algorithm only accounts for about 10% of the total execution time of the entire drive control program. In summary, the proposed VG-LADRC controller has low resource occupancy and good algorithm execution efficiency while maintaining excellent control performance and adaptability.

B. Convergence Performance of the Estimated Control Gain

As shown in Fig. 12, in order to further verify the convergence performance of the proposed control gain adaptive law, a trapezoidal speed command is used to conduct a comparative experiment between the ETSO-based controller and VG-LADRC. In the experiment, the speed change cycle is increased to extend the steady-state operation time of the motor. The experimental condition settings are shown in Table II.

Under the condition of clutch separation, the tested motor has no load, and the output value of the motor controller is small. The initial value of the estimated control gain in the controller is set to 800. The motor speed control waveforms under the two control methods are shown in Fig. 12. The convergence results of the estimated control gain are shown in Fig. 13. The setting of the adaptive threshold φ ensures that the control gain adaptive law is only activated during the dynamic operation of the motor, thereby maximally balancing dynamic response and steady-state accuracy. Based on the different excitation conditions for the convergence of the estimated control gain in the two methods, the flag CS is set to show the convergence status of the estimated control gain. When the convergence condition is met, $CS = 1$; otherwise, $CS = 0$. As can be seen from Fig. 12, both compared methods have a certain degree of robustness. When the motor speed is constant, the convergence status of each control gain is zero $CS = 0$, which ensures the stability of the estimated control gain. When the motor speed changes, the control gain convergence status $CS = 1$, ensuring that it converges to the actual value.

By analyzing the control gain convergence state waveform when the motor speed changes, as shown in Fig. 12, it can be seen that the time for the proposed VG-LADRC to satisfy the convergence condition $CS = 1$ during the same dynamic change process is significantly more than that of the ETSO-based controller. The VG-LADRC only needs three trapezoidal speed cycles to converge to 359.2, with a convergence error of 3.3%. However, the ETSO-based controller cannot even converge the estimated control gain to the vicinity of the actual value (347.6) during the entire test process. With further convergence, the control gain convergence average value in the VG-LADRC is 351, and its convergence error is less than 1%. Comparing the speed tracking waveforms, it can be seen that, when the control gain is mismatched, the motor speed under the proposed controller does not have overshoot and speed lag.

In addition, the same comparative experiment is conducted when the motor is loaded. The convergence results of the estimated control gain are shown in Fig. 14. In the first speed cycle, the estimated control gain convergence process of the two methods accounts for 76.0% and 65.4% of the estimated control

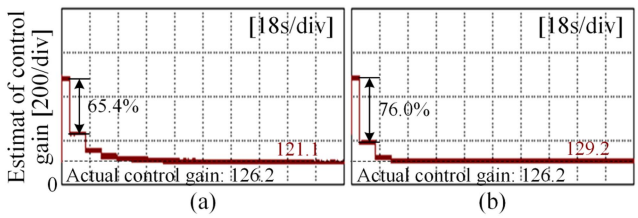

Fig. 14. Convergence results of the estimated control gain under load. (a) ETSO-based speed controller. (b) VG-LADRC.

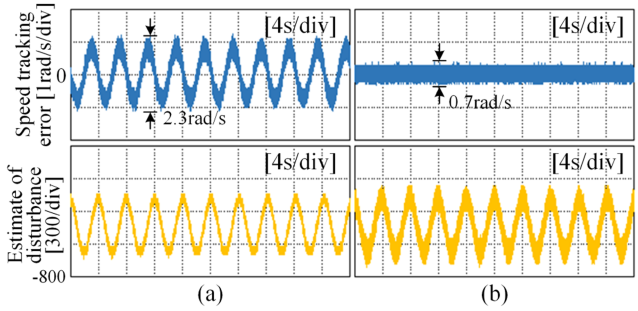

Fig. 15. Speed tracking errors under sinusoidal load. (a) ETSO-based speed controller. (b) VG-LADRC.

gain difference (between the initial value and the actual value). The convergence dynamic performance of the control gain in the VG-LADRC is still better than that of the ETSO-based controller. In the convergence stability stage, both methods can make the estimated control gain converge to its actual value, and the convergence error does not exceed 2% and 4% of the actual value, with high convergence accuracy.

C. Disturbance Suppression Performance of Control System

This article conducts a comparative experiment of sinusoidal loading to compare the disturbance suppression performance of VG-LADRC and ETSO-based controller. The speed command is set to 100 rad/s. During the loading process, the control gain convergence state of the two controllers is always zero, and the control gain in the controller is a constant value near the actual value. The observed lumped disturbance and speed tracking error waveforms of the two methods under sinusoidal loading are shown in Fig. 15. Comparing Fig. 15(a) with (b), the disturbance information in the lumped disturbance observed by the proposed VG-LADRC is significantly more than that of the ETSO-based controller. In addition, the motor speed under the control of the ETSO-based controller is obviously more susceptible to external load changes, showing the same sinusoidal speed fluctuation as the load waveform, about 2.3 rad/s. The motor speed under VG-LADRC control is almost unaffected, and the fluctuation error is about one-third of the former (0.7 rad/s). It should be noted that the speed tracking error waveform output by the external digital-to-analog converter (DAC) chip is inevitably affected by environmental noise, and the actual speed tracking error amplitude is smaller than that shown in the waveform.

V. Conclusion

This article proposes a VG-LADRC speed controller with strong anti-interference ability and control gain adaptive characteristics to achieve high-performance speed control of PMSM-drive system. The proposed controller is experimentally verified on an experimental platform that can meet the simultaneous changes of load torque and control gain. The main contributions of this article include the following:

1) This article proposes a VG-LADRC control structure with a CESO. ESO1 can realize the joint estimation of external disturbance and system control gain, and ESO2 can perform in-depth estimation of residual disturbance on this basis. The collaborative operation between the two-level observers effectively improves the dynamic response capability and disturbance suppression capability of the system.
2) Aiming at the problem that the control gain of the actual system changes with the operating conditions, this article designs a control gain adaptive law based on error feedback. It can realize the online estimation and dynamic adjustment of the control gain, avoid the performance degradation problem that may be caused by the fixed control gain in the traditional LADRC, and significantly enhances the control system's adaptive ability to parameter uncertainty.
3) The design of the control gain adaptive factor based on the motor dynamic information and speed tracking error enables the controller to capture more details of the motor operation information to dynamically adjust the convergence speed and steady-state accuracy of the control gain, greatly improving the robustness of the convergence of the estimated control gain under complex working conditions.
4) Through theoretical derivation and frequency-domain analysis, the proposed VG-LADRC control structure has significant advantages in low-frequency disturbance suppression while maintaining good performance under medium- and high-frequency disturbances. In particular, the controller has higher robustness to control gain mismatch. When the control gain is mismatched, its low-frequency disturbance suppression performance is almost unaffected, and its high-frequency disturbance suppression capability only changes slightly, reflecting strong engineering adaptability.

References

[1] P. Chen, H. Gan, Y. Liu, and Y. Luo, "Different model-based ADRCs satisfying performance independent control for PMSM speed servo system," *IEEE Trans. Ind. Electron.*, vol. 72, no. 2, pp. 2012–2023, Feb. 2025.
[2] Z. Lyu, L. Wu, and P. Song, "A novel harmonic current control method for torque ripple reduction of SPMSM considering DC-link voltage limit," *IEEE Trans. Power Electron.*, vol. 39, no. 2, pp. 2558–2568, Feb. 2024.
[3] Q. Hou et al., "Enhanced active disturbance rejection control with measurement noise suppression for PMSM drives via augmented nonlinear extended state observer," *IEEE Trans. Energy Convers.*, vol. 39, no. 1, pp. 287–299, Mar. 2024.
[4] B. Wang, M. Tian, Y. Yu, Q. Dong, and D. Xu, "Enhanced ADRC with quasi-resonant control for PMSM speed regulation considering aperiodic and periodic disturbances," *IEEE Trans. Transp. Electrific.*, vol. 8, no. 3, pp. 3568–3577, Sep. 2022.

[5] L. Wang, Z. Tang, P. Zhang, X. Liu, D. Wang, and X. Li, "Double extended sliding-mode observer-based synchronous estimation of total inertia and load torque for PMSM-driven spindle-tool systems," *IEEE Trans. Ind. Inform.*, vol. 19, no. 7, pp. 8496–8507, Jul. 2023.
[6] Q. Hou and S. Ding, "Finite-time extended state observer-based super-twisting sliding mode controller for PMSM drives with inertia identification," *IEEE Trans. Transp. Electrific.*, vol. 8, no. 2, pp. 1918–1929, Jun. 2022.
[7] T. Shi, S. Lin, Y. Cao, and Y. Yan, "A two-degree-of-freedom explicit model predictive non-cascaded direct speed control for SPMSM drives," *IEEE Trans. Transp. Electrific.*, vol. 11, no. 1, pp. 510–520, Feb. 2025.
[8] Y. Zuo, J. Mei, C. Jiang, X. Yuan, S. Xie, and C. H. T. Lee, "Linear active disturbance rejection controllers for PMSM speed regulation system considering the speed filter," *IEEE Trans. Power Electron.*, vol. 36, no. 12, pp. 14579–14592, Dec. 2021.
[9] Q. Hou, Y. Zuo, J. Sun, C. H. T. Lee, Y. Wang, and S. Ding, "Modified nonlinear active disturbance rejection control for PMSM speed regulation with frequency domain analysis," *IEEE Trans. Power Electron.*, vol. 38, no. 7, pp. 8126–8134, Jul. 2023.
[10] H. Wu, C. Gan, H. Wang, S. Wang, R. Qu, and X. Liu, "Active disturbance rejection speed control with double-stage-ESO considering aperiodic and periodic disturbances for PMSM drives," *IEEE Trans. Ind. Electron.*, to be published, doi: 10.1109/TIE.2024.3519622.
[11] C. Wang, J. Yan, P. Heng, L. Shan, and X. Zhou, "Enhanced LADRC for permanent magnet synchronous motor with compensation function observer," *IEEE J. Emerg. Sel. Topics Power Electron.*, vol. 11, no. 3, pp. 3424–3434, Jun. 2023.
[12] C. Liu, G. Luo, X. Duan, Z. Chen, Z. Zhang, and C. Qiu, "Adaptive LADRC-based disturbance rejection method for electromechanical servo system," *IEEE Trans. Ind. Appl.*, vol. 56, no. 1, pp. 876–889, Jan. 2020.
[13] S. Tang, T. Shi, C. Li, Y. Cao, and Z. Wang, "An enhanced linear active disturbance rejection speed controller for PMSMs," in *Proc. 12th Int. Conf. Power Electron., Mach. Drives*, 2023, pp. 65–71.
[14] G. Wang, R. Liu, N. Zhao, D. Ding, and D. Xu, "Enhanced linear ADRC strategy for HF pulse voltage signal injection-based sensorless IPMSM drives," *IEEE Trans. Power Electron.*, vol. 34, no. 1, pp. 514–525, Jan. 2019.
[15] S. Lin, Y. Cao, C. Li, Z. Wang, T. Shi, and C. Xia, "Two-degree-of-freedom active disturbance rejection current control for permanent magnet synchronous motors," *IEEE Trans. Power Electron.*, vol. 38, no. 3, pp. 3640–3652, Mar. 2023.
[16] P. Lin, Z. Wu, K.-Z. Liu, and X.-M. Sun, "A class of linear–nonlinear switching active disturbance rejection speed and current controllers for PMSM," *IEEE Trans. Power Electron.*, vol. 36, no. 12, pp. 14366–14382, Dec. 2021.
[17] Z. Hao et al., "Linear/nonlinear active disturbance rejection switching control for permanent magnet synchronous motors," *IEEE Trans. Power Electron.*, vol. 36, no. 8, pp. 9334–9347, Aug. 2021.
[18] Y. Zuo, X. Zhu, L. Quan, C. Zhang, Y. Du, and Z. Xiang, "Active disturbance rejection controller for speed control of electrical drives using phase-locking loop observer," *IEEE Trans. Ind. Electron.*, vol. 66, no. 3, pp. 1748–1759, Mar. 2019.
[19] F. Jiang, F. Yang, S. Sun, and K. Yang, "Improved linear active disturbance rejection control for IPMSM drives considering load inertia mismatch," *Energies*, vol. 15, no. 3, Jan. 2022, Art. no. 1169.
[20] S. Li and Z. Liu, "Adaptive speed control for permanent-magnet synchronous motor system with variations of load inertia," *IEEE Trans. Ind. Electron.*, vol. 56, no. 8, pp. 3050–3059, Aug. 2009.
[21] H. Liu, D. Tian, Y. Wang, H. Liu, S. Zhao, and Z. Wu, "Model-compensated active disturbance rejection control for PMSM based on parameters identification," in *Proc. 8th Int. Conf. Robot., Control Automat.*, 2024, pp. 318–324.
[22] S. Tang, T. Shi, Y. Cao, Z. Lin, Z. Wang, and Y. Yan, "Simultaneous identification of load torque and moment of inertia of PMSM based on variable structure extended sliding mode observer," *IEEE Trans. Power Electron.*, vol. 39, no. 7, pp. 8585–8596, Jul. 2024.
[23] J. Xiong and X. Fu, "Extended two-state observer-based speed control for PMSM with uncertainties of control input gain and lumped disturbance," *IEEE Trans. Ind. Electron.*, vol. 71, no. 6, pp. 6172–6182, Jun. 2024.
[24] Y. Fei, P. Shi, and C.-C. Lim, "Robust and collision-free formation control of multiagent systems with limited information," *IEEE Trans. Neural Netw. Learn. Syst.*, vol. 34, no. 8, pp. 4286–4295, Aug. 2023.

Shuaipeng Tang was born in Hebei, China, in 1995. He received the B.S. degree in electrical engineering from the College of Electrical Engineering, Hebei University of Technology, Tianjin, China, in 2020. He is currently working toward the Ph.D. degree in electrical engineering with the College of Electrical Engineering, Zhejiang University, Hangzhou, China.

His research interests include electrical machines, servo motor drives, and power electronics.

Tingna Shi (Senior Member, IEEE) was born in Yuyao, China, in 1969. She received the B.S. and M.S. degrees from Zhejiang University, Hangzhou, China, in 1991 and 1996, respectively, and the Ph.D. degree from Tianjin University, Tianjin, China, in 2009, all in electrical engineering.

She is currently a Professor with the College of Electrical Engineering, Zhejiang University. Her current research interests include electrical machines and their control systems, power electronics, and electric drives.

Yanfei Cao (Member, IEEE) was born in Hebei, China, in 1990. She received the B.S. degree in automation from the Hebei University of Technology, City College, Tianjin, China, in 2013, and Ph.D. degree in control science and engineering from Tianjin University, Tianjin, China, in 2019.

She is currently an Associate Researcher with the College of Electrical Engineering, Zhejiang University, Hangzhou, China. Her research interests include electrical machines, motor drives, and power electronics.

Yan Yan was born in Tianjin, China, in 1981. She received the B.S. and M.S. degrees from the Tianjin University of Science and Technology, Tianjin, China, in 2004 and 2007, respectively, and the Ph.D. degree from Tianjin University, Tianjin, China, in 2010, all in electrical engineering.

She is currently a Professor with the College of Electrical Engineering, Zhejiang University, Hangzhou, China, and also works with Zhejiang University Advanced Electrical Equipment Innovation Center, Hangzhou, China. Her current research interests include electrical machines and their control systems, power electronics, and electric drives.

Changliang Xia (Senior Member, IEEE) was born in Tianjin, China, in 1968. He received the B.S. degree from Tianjin University, Tianjin, China, in 1990, and the M.S. and Ph.D. degrees from Zhejiang University, Hangzhou, China, in 1993 and 1995, respectively, all in electrical engineering.

He was elected Academician of the Chinese Academy of Engineering in 2017. He is a Researcher with Zhejiang University Advanced Electrical Equipment Innovation Center, Hangzhou, China, and also a Professor with Tiangong University, Tianjin, China. He is currently the Qiushi Chair Professor with Zhejiang University. His research interests include electrical machines, power electronics, and their control systems.